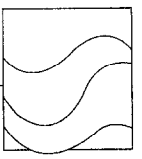

A 2-D section of ^{228}Ra and ^{226}Ra in the Northeast Pacific

Chih-An HUH [a], Teh-Lung KU [b]

[a] Institute of Earth Sciences, Academia Sinica, P.O. Box 1-55, Nankang, Taipei, Taiwan, ROC
[b] Department of Geological Sciences, University of Southern California, Los Angeles, CA 90089-0740, USA

(Received 28/02/97, revised 25/11/97, accepted 09/12/97)

Abstract – Seawater samples collected in the northeast Pacific from 112° 50'W to 126° 36'W along a latitudinal band (21–25° N) have been analysed for ^{228}Ra and ^{226}Ra. Both nuclides exhibit their characteristic distributions. In the surface water, the exponential-like decrease of ^{228} Ra away from Baja California can be interpreted by horizontal water mixing with eddy diffusion coefficients (K_x) of 1×10^6 cm^2 s^{-1} and 5×10^7 cm^2 s^{-1} for scale lengths of 200 km and 1000 km, respectively. In the bottom waters, the decrease of ^{228}Ra away from bottom sediments can be modeled by vertical eddy diffusivities (K_z) of 15–30 cm^2 s^{-1} except at one station (24° 16.9' N, 115° 8.9' W) where a value of 120 cm^2 s^{-1} is obtained. The ^{228}Ra-derived diffusivities were used to compute the mass balance of ^{226}Ra using a two-box model. The model results show a mean mixing coefficient of 3.8 cm^2 s^{-1} for the thermocline and a mean upwelling velocity of 7.7 m y^{-1} in the study area, both are about two or three times higher than those generally quoted for the Pacific. © Elsevier, Paris

radium-228 / radium-226 / eddy diffusion / Northeast Pacific

Résumé – Un profil bidimensionnel de ^{228}Ra et ^{226}Ra dans la région Nord-Est du Pacifique. Une étude de deux isotopes du radium (^{226}Ra et ^{228}Ra) a été menée sur des échantillons d'eau de mer prélevés dans le Nord-Est Pacifique, dans une zone comprise entre les méridiens 112° 50' W et 126° 36' W et entre les parallèles 21° N et 25° N. Les distributions caractéristiques se retrouvent pour les deux isotopes. On note à la surface de la mer, au large de la Basse Californie, une décroissance exponentielle du ^{228}Ra ; elle pourrait provenir d'un brassage horizontal des eaux, avec des coefficients de diffusion turbulente (K_x) de 1×10^6 cm^2 s^{-1} pour une distance de 200 km et de 5×10^7 cm^2 s^{-1} pour 1000 km. À la base des eaux, la décroissance du ^{228}Ra en fonction de l'éloignement des sédiments peut être restituée par un coefficient de diffusion turbulente verticale (K_z) de 15 à 30 cm^2 s^{-1}, sauf à une station (24° 16,9'N, 115° 8,9'W), où l'on obtient une valeur de 120 cm^2 s^{-1}. Les coefficients de diffusion du ^{228}Ra servent à déterminer, d'après un modèle à deux boîtes, le bilan des masses avec le ^{226}Ra. Les résultats du modèle montrent un brassage moyen de 3,8 cm^2 s^{-1} pour la thermocline et une vitesse moyenne de remontée d'eau marine de 7,7 m a^{-1} dans la zone étudiée. Les deux valeurs sont deux à trois fois plus élevées que celles habituellement observées dans le Pacifique. © Elsevier, Paris

radium 228 / radium 226 / diffusion turbulente / Nord-Est Pacifique

1. INTRODUCTION

That there exists an excess of ^{228}Ra (half-life = 5.75 y) relative to ^{232}Th in seawater was suggested three to four decades ago by the discovery of ^{232}Th-^{228}Th disequilibrium in the oceans [7, 18, 21] and confirmed later by the first direct measurements of ^{228}Ra in seawater by Moore [13]. Subsequent studies [4, 14, 15, 22] documented that ^{228}Ra decreased horizontally away from the coasts, and vertically away from the seafloor. These observations reflect the fact that ^{228}Ra was supplied from the decay of ^{232}Th in marine sediments and transported away from its source regions by eddy mixing. Consequently, many attempts have been made to determine oceanic mixing rates using the distribution of this nuclide [4, 6, 20, 23].

As with ^{228}Ra, the primary source of ^{226}Ra (half-life = 1,622 y) is also bottom sediments, especially the slowly

accumulated pelagic sediments with enriched ^{230}Th (the progenitor of ^{226}Ra). Using Ba as a stable analogue for radioisotopes of Ra, attempts have been made to apply ^{226}Ra as a tracer for studying large-scale oceanic circulation and mixing in the deep sea [3, 8, 9].

Although ^{228}Ra and ^{226}Ra have similar source terms and their distributions in the water column are controlled by the same processes, the two isotopes have rarely been measured concurrently. This is due in part to the fact that they can be used independently from each other in different oceanic regimes, and in part to the difference in analytical methods and sample sizes required for their analysis. On the other hand, data available for both nuclides could provide information regarding water mixing in a given oceanic area additional to that derived from the use of either nuclide alone.

In this paper, a two-dimensional section of ^{228}Ra and ^{226}Ra in the east Pacific is presented. We use the ^{228}Ra data to derive mixing rates in bottom and surface waters. The results are then applied to the mass balance for ^{226}Ra showing that relatively intense vertical mixing may occur in the area which aids in the export of ^{226}Ra to other parts of the Pacific Ocean.

In deducing the mixing rates, we are aware of the pitfalls of ignoring the three dimensionality of the ocean by assuming a negligibly small Ra concentration gradient in the N–S (y) direction relative to those of the x and z directions. This simplification, while being necessary due to the lack of data, may be justified because of the source function of Ra is largely two dimensional in nature: shelf sediments as a source for horizontal offshore dispersion in surface ocean and deep-sea sediments as a source for vertical mixing in the deep ocean. In other words, vertical and offshore gradients are much larger than along-shore gradients for Ra. If the eddy diffusion coefficients do not significantly differ in the x and y directions, then the along-shore transport of Ra (especially for the short-lived ^{228}Ra) may be omitted. Treating the distribution of ^{228}Ra in the surface open ocean as quasi-one dimensional appears further tolerable, since the shelf source of ^{228}Ra is effectively isolated from its deep-sea source. However, we will examine this aspect later.

2. MATERIALS AND METHODS

Samples for ^{226}Ra and ^{228}Ra analyses were collected at seven stations (stations 3, 4, 5, 6, 7, 8 and 10) aboard R/V Thomas G. Thompson during cruise TT-145 in October 1979. The cruise track, from Hawaii (156° W) to Mazatlan, Mexico (112° W), was confined within the 21–25° N latitudinal band (*figure 1*).

For sampling the deep-water ^{228}Ra, acrylic fibres impregnated with MnO_2 were used to concentrate Ra isotopes in-situ from large volumes of seawater [17] as follows. About 100 g of Mn fibre was put in a Nylon net bag and tied inside a Niskin sampler. Six such samplers were attached, one by one, to the ship's hydrowire at pre-determined intervals (hence water column depths) when the wire was paid out. During the descent of the Niskin bottles, their end caps were corked open. To prevent collection of Ra isotopes by the fibres from upper parts of the water column, each Nylon bag was wrapped in a plastic sheet and tied by a rubber band with a stick pencil ($MgSO_4$) link. Upon total dissolution and release of the link, the plastic sheet was floated away, exposing the acrylic fibre to seawater at desired depths. In order to facilitate the contact of a large volume of seawater with the fibres, the entire hydrocast wire was repeatedly lifted up 10 m and then lowered down 10 m. At the conclusion of this "yo-yo" motion which lasted 2–4 h at each station, a messenger was sent down the wire to close the Niskin bottles for sample recovery. In addition to the six deep-water samples collected from the hydrocast, a surface sample was collected by running seawater through a cartridge packed with Mn fibre and connected to the ship's saltwater line. Thus, each profile measured consists of seven data points. The uncertainty of the sampling depth due to the up-and-down motion (within ± 10 m) is sufficiently small relative to the vertical spacing (> 100 m) between samples in the water column.

In conjunction with the fibre samples, 20 L seawater samples were collected, using Niskin bottles, from the water column for the determination of ^{226}Ra (via ^{222}Rn) as an internal tracer to derive the "effective volume" collected by the fibre adsorbers.

In the laboratory, the Mn fibres were leached with 4N HCl in the presence of H_2O_2. The leachate was evaporated to dryness and taken to 8N HNO_3. Thorium isotopes initially present in the samples were removed by passing the 8N HNO_3 sample solution through an anion exchange column (Dowex AG1 × 8) twice. A small aliquot of the sample solution was then taken for the determination of ^{226}Ra by the ^{222}Rn emanation method [5]. The remaining solution was spiked with ^{229}Th and stored for three years for the ingrowth of ^{228}Th from ^{228}Ra. Activities of ^{228}Ra in the fibre leachates were then determined via ^{228}Th by alpha spectrometry.

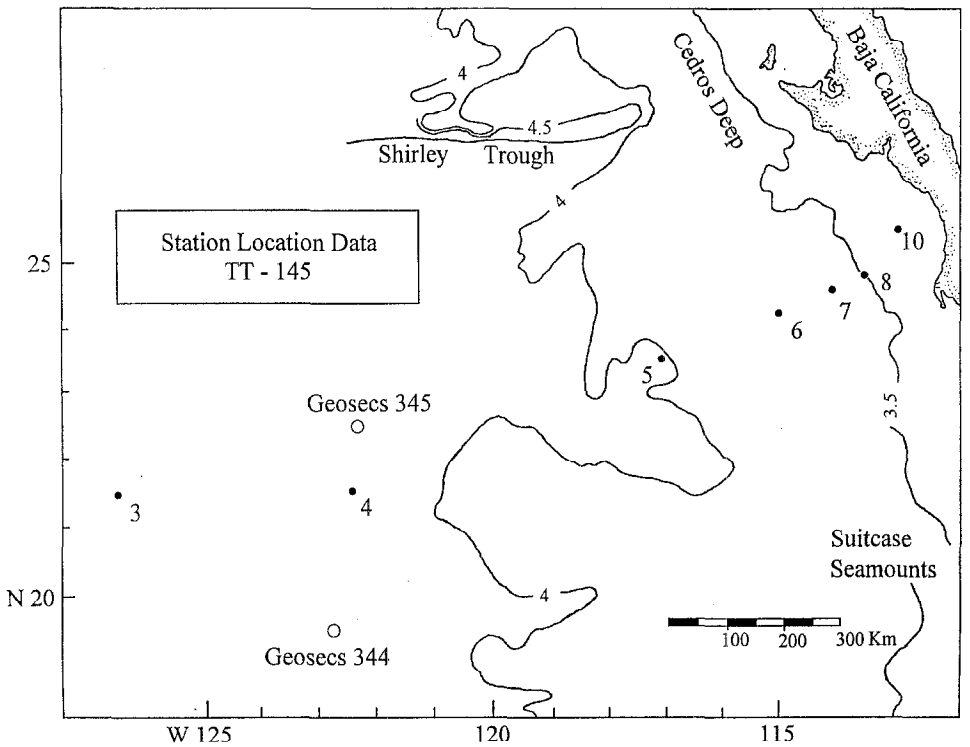

Figure 1. Map showing the seven sites sampled for ^{228}Ra and ^{226}Ra measurements.

3. RESULTS AND DISCUSSION

Multiplying the ^{228}Ra/^{226}Ra activity ratio from Mn fibres by the concentration of ^{226}Ra (dpm 100 kg^{-1}) determined from the 20 L samples yields the concentration of ^{228}Ra. In several instances the sampling depths of the 20 L samples do not coincide precisely with those of the fibre samples. In such cases the ^{226}Ra concentration was determined by linear interpolation of the profile data. The measured, interpolated and calculated data are listed in *Table I.* The uncertainties quoted are ± 1 σ based on counting statistics and propagation of errors during calculation.

3.1. Distribution of ^{228}Ra and ^{226}Ra

Water column profiles of ^{226}Ra at all stations are fairly similar and exhibit the typical trend of increasing with depth, from 7–8 dpm 100 kg^{-1} at surface to > 40 dpm 100 kg^{-1} at depth (*figure 2a*). There is some indication of a "plume" of ^{226}Ra-rich bottom water moving upward near station 6 (*figure 2b*).

The ^{228}Ra/^{226}Ra activity ratios vary between 0.003–0.15, well within the range observed in the Pacific Ocean. The lowest ^{228}Ra/^{226}Ra ratio, 0.0005, was found in intermediate waters at the JGOFS equatorial Pacific sites [10], and the highest ratio, 0.3, was observed in coastal waters off Callao, Peru [6]. The highest value we measured at station 10 (0.154 ± 0.007), in coastal water ~ 50 miles off Baja California, is similar to those (0.16–0.23) reported by Kaufman et al. [4] for other nearby sites.

Our measured ^{228}Ra activities also compare favourably with those reported previously for adjacent locations. For instance, our surface water ^{228}Ra activities at station 4 (0.6 dpm 100 kg^{-1}) and station 7 (1.2 dpm 100 kg^{-1}) agree well with those at GEOSECS station 345 (0.5 dpm 100 kg^{-1}; [14]) and off Mexican coast (1.0–1.3 dpm 100 kg^{-1}; [6]), respectively.

Figure 3 shows the profiles of ^{228}Ra at stations 3, 4, 5, 6 and 7, which all show higher values in surface and bottom waters relative to those at mid-depths. In the surface ocean, there is decreasing trend from the coast toward the open ocean. The data set adds to previous observations on the general distribution pattern of ^{228}Ra concentrations in the ocean: near-shore waters > open-ocean surface waters > open-ocean subsurface waters < near-bottom water [4, 14].

Table I. Isotopic data of Ra in Mn fiber and 20-l seawater sampled during TT-145 cruise.

Depth (m)	$^{228}Ra/^{226}Ra$ ($\times 10^{-2}$)	^{226}Ra (dpm/100 kg)	$^{228}Ra^*$ (dpm/100 kg)
Station 3 (21° 26.7′ N, 126° 36.0′ W)			
0	4.16 ± 0.58	7.6 ± 0.2	0.32 ± 0.04
500	–	14.2 ± 0.3	–
1000	0.30 ± 0.05	20.7 ± 0.4	0.06 ± 0.01
1500	–	25.2 ± 0.5	–
2000	–	29.6 ± 1.5	–
2500	–	32.5 ± 0.2	–
3000	0.30 ± 0.03	36.8 ± 0.7	0.11 ± 0.01
3500	0.37 ± 0.02	41.4 ± 0.6	0.15 ± 0.01
4000	0.94 ± 0.09	41.7 ± 1.8	0.39 ± 0.04
4500	2.11 ± 0.20	45.7 ± 1.4	0.96 ± 0.10
4750	2.40 ± 0.22	*47.0*	1.13 ± 0.10
Station 4 (21° 36.3′ N, 122° 21.4′ W)			
0	3.84 ± 0.31	7.8 ± 0.2	0.30 ± 0.03
500	–	15.0 ± 0.3	–
1000	0.69 ± 0.07	21.6 ± 0.5	0.15 ± 0.02
1500	–	26.4 ± 1.2	–
1900	–	28.3 ± 1.0	–
2300	–	35.2 ± 0.8	–
2700	–	34.4 ± 1.1	–
3000	0.99 ± 0.07	*38.8*	0.38 ± 0.03
3100	–	40.2 ± 1.0	–
3250	1.18 ± 0.17	*41.4*	0.49 ± 0.07
3500	1.38 ± 0.11	43.4 ± 0.5	0.60 ± 0.05
3750	1.41 ± 0.09	*43.7*	0.62 ± 0.04
4000	2.84 ± 0.20	44.0 ± 1.0	1.25 ± 0.09
Station 5 (23° 30.1′ N, 116° 57.4′ W)			
0	4.51 ± 0.59	8.7 ± 0.2	0.39 ± 0.05
500	–	19.8 ± 0.3	–
1000	0.61 ± 0.08	24.6 ± 0.4	0.15 ± 0.02
1500	–	31.5 ± 0.4	–
1900	–	31.2 ± 0.8	–
2300	–	34.4 ± 1.3	–
2700	–	39.1 ± 1.0	–
3000	0.31 ± 0.04	*39.0*	0.12 ± 0.02
3100	–	39.0 ± 1.1	–
3250	0.80 ± 0.06	*40.4*	0.32 ± 0.02
3500	0.75 ± 0.11	42.7 ± 0.8	0.32 ± 0.05
3750	0.84 ± 0.08	*42.7*	0.36 ± 0.03
3900	–	42.7 ± 0.7	–
4000	1.96 ± 0.17	43.8 ± 0.7	0.86 ± 0.08
Station 6 (24° 16.9′ N, 115° 08.9′ W)			
0	5.47 ± 0.70	8.6 ± 0.3	0.47 ± 0.06
500	–	17.5 ± 0.3	–
1000	0.79 ± 0.08	21.0 ± 0.5	0.17 ± 0.02
1500	–	30.1 ± 1.0	–
2000	–	33.2 ± 1.1	–
2500	–	38.3 ± 1.2	–
2850	0.46 ± 0.04	*39.5*	0.18 ± 0.02
3000	–	40.0 ± 1.0	–
3100	0.40 ± 0.03	*40.3*	0.16 ± 0.01
3350	0.40 ± 0.04	*41.1*	0.16 ± 0.02
3500	–	41.6 ± 0.8	–
3600	0.54 – 0.04	*42.0*	0.23 ± 0.02
3750	–	42.5 ± 0.7	–
3850	0.72 ± 0.06	*43.0*	0.31 ± 0.03
Station 7 (24° 41.9′ N, 113° 58.3′ W)			
0	7.08 ± 0.95	8.5 ± 0.5	0.60 ± 0.09
700	–	18.9 ± 0.7	–
1100	–	23.2 ± 0.7	–
1180	0.57 ± 0.06	*24.2*	0.14 ± 0.01
1900	–	32.8 ± 1.2	–
2300	–	35.9 ± 0.4	–
2680	0.41 ± 0.03	*38.1*	0.16 ± 0.01
2930	0.54 ± 0.04	*39.6*	0.21 ± 0.02
3100	–	40.6 ± 0.4	–
3180	0.84 ± 0.07	*40.5*	0.34 ± 0.03
3430	1.11 ± 0.11	*40.3*	0.45 ± 0.04
3550	–	40.2 ± 1.4	–
3680	1.21 ± 0.12	*40.2*	0.49 ± 0.05
Station 8 (24° 56.6′ N, 113° 24.2′ W)			
0	8.70 ± 0.51	8.2 ± 0.3	0.71 ± 0.05
Station 10 (25° 37.5′ N, 112° 50.0′ W)			
0	15.4 ± 1.0	8.0 ± 0.2	1.23 ± 0.09

Errors for ^{226}Ra data are one standard deviation based on counting statistics or three replicate measurements, whichever is larger.
* The ^{228}Ra activities are calculated from the $^{228}Ra/^{226}Ra$ activity ratios observed in Mn fibers (column 2) and the ^{226}Ra in 20-liter seawater samples (column 3).
Where no direct measurements of ^{226}Ra were made, the ^{226}Ra activities, as shown in italics, were estimated by interpolation.

3.2. ^{228}Ra distribution in the surface water - Horizontal eddy diffusivity

^{228}Ra in the surface ocean is primarily produced in continental shelf sediments from the decay of ^{232}Th. ^{228}Ra tends to diffuse from sediment pore waters into the overlying shelf water after its production. Horizontal mixing transports ^{228}Ra in the surface mixed layer offshore into the open ocean. Earlier studies [4, 6] have shown that the offshore horizontal distribution of ^{228}Ra in the surface ocean under steady state can be described by:

$$K_x \frac{\partial^2 C}{\partial X^2} - \lambda C = 0 \qquad (1)$$

where x = horizontal distance offshore; C = concentration of ^{228}Ra; λ is the decay constant of ^{228}Ra; and K_x is the apparent horizontal eddy diffusivity. Solving under the

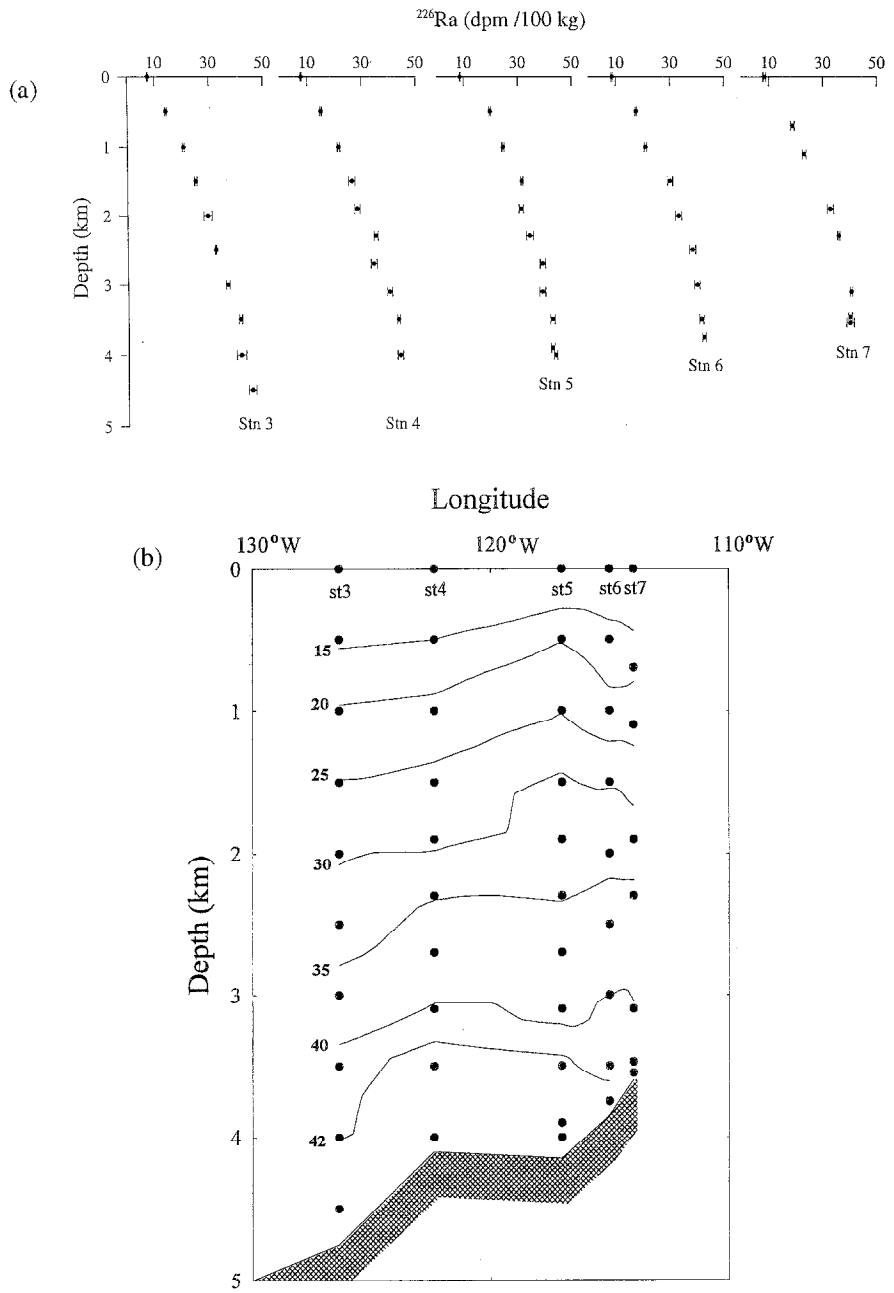

Figure 2. (a) Water column profiles and (b) cross section of ^{226}Ra at deep stations (stations 3–7) along the TT-145 cruise track.

boundary condition of $C = C_0$ at $x = 0$, and $C = 0$ at $x = \infty$ we have:

$$C = C_0 \exp(-\sqrt{\lambda / K_x} X) \qquad (2)$$

Plotted in *figure 4* are our measured C as a function of x for surface water samples in the eastern Pacific along the 21–25° N latitudinal band. Fitting to the exponential function of equation (2) gives K_x for the surface ocean in the region. Horizontal mixing is affected by the length scale of the turbulent eddy motion, or size of the eddies [19]. The *figure 4* results indicate two regimes with different characteristic mixing lengths. The outer stations (4, 5, 6, and 7) appear to fall in a regime with a K_x of 5 ×

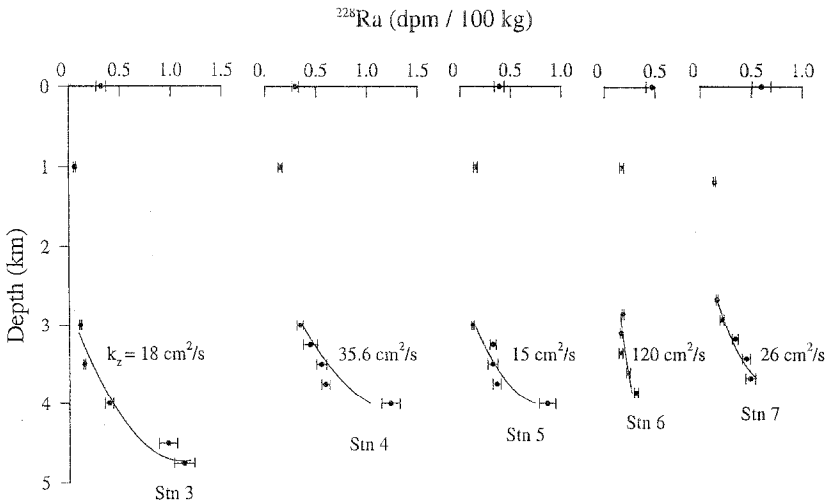

Figure 3. Water column distribution of ^{228}Ra at stations 3–7. Apparent vertical eddy diffusion coefficients in bottom waters derived from ^{228}Ra gradients are indicated.

10^7 cm^2 s^{-1}, whereas the inner stations (7, 8 and 10) are located in a different mixing domain with K_x of 1 × 10^6 cm^2 s^{-1}. These values and their corresponding scale lengths are compatible with those reported previously [4, 6, 23].

It should be pointed out, however, that Lapacian diffusion may not apply to horizontal mixing as it may involve advective motion depending on length scales of observation. For this reason we named K_x derived earlier as the "apparent" horizontal eddy diffusion coefficient. In the analysis that follows, we show that whereas advection may play a role, for lack of detailed near-surface vertical ^{228}Ra profiles, the apparent diffusivity deduced via the equation (1) approach remains a viable parameter in

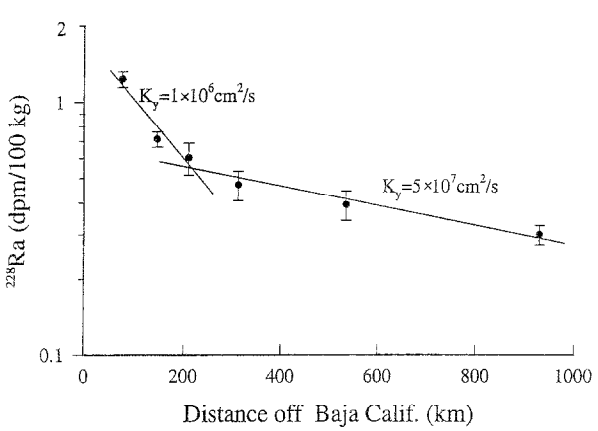

Figure 4. Plot of ^{228}Ra in surface water versus distance from coast. Solid lines correspond to horizontal eddy diffusion coefficients calculated from the gradients.

describing the horizontal ^{228}Ra distribution in the study area.

Let K_x' be the horizontal eddy diffusivity which does not incorporate the effect of advection. We rewrite equation (1) as

$$\frac{\partial}{\partial X}\left(K_x' \frac{\partial C}{\partial X}\right) - \left(\omega_x \frac{\partial C}{\partial X}\right) - \lambda C = 0 \qquad (3)$$

where ω_x is the advective velocity, positive being the offshore direction. From (1) and (3) it can be seen from the relationship below that the apparent horizontal eddy diffusivity, K_x, depends on K_x', ω_x, and C (hence K_x derived from the ^{228}Ra distribution may differ from K_x derived from the ^{226}Ra distribution, depending on the magnitude of ω_x):

$$K_x = K_x'\left[1 - \left(\frac{\omega_x}{K_x'}\right)\left(\frac{\partial \ln C}{\partial X}\right)^{-1}\right] \qquad (4)$$

If the current is of offshore direction ($\omega_x > 0$), $K_x > K_x'$ and for onshore currents ($\omega_x < 0$), $K_x < K_x'$. How large would be the advection before K_x differs significantly from K_x', say, by a factor of two ? To answer, we rearrange (4) to write:

$$\omega_x = -\left(\frac{K_x}{K_x'} - 1\right)\left(\frac{\partial \ln C}{\partial X}\right)K_x' \qquad (5)$$

The term $\partial \ln C/\partial x$ in the equation can be evaluated from the observed ^{228}Ra distribution (*figure 4*), giving values of -8.5×10^{-4} and -0.8×10^{-5} km^{-1} for the outer and inner sections, respectively. Substituting these values into

equation (5) and letting $K_x/K'_x = 2$, we have ω_x = 0.22 cm s^{-1} and $K'_x = 2.5 \times 10^7$ cm^2 s^{-1} for the outer-station mixing regime, and ω_x = 0.027 cm s^{-1} and $K'_x = 0.5 \times 10^6$ cm^2 s^{-1} for the inner-station regime. For K_x/K'_x = 0.5, the corresponding combinations are ω_x = -0.11 cm s^{-1} and $K'_x = 1 \times 10^8$ cm^2 s^{-1}, and ω_x = –0.014 cm s^{-1} and $K'_x = 2 \times 10^6$ cm^2 s^{-1}. The small magnitude of the ω_x values thus derived points to the sensitivity of advection in influencing the ^{228}Ra distribution. As a positive ω_x (offshore advection) is likely to apply for the study area, the apparent diffusivity K_x shown in *figure 4* could be higher than K'_x, the horizontal diffusivity in the true Lapacian sense. However, the exponential decreases (or the slopes) of the ^{228}Ra plots in *figure 4* could well be influenced by vertical mixing as well. The effect of the vertical mixing is such that it steepens the horizontal gradient, making the apparent diffusivity K_x lower than K'_x. This is because in surface ocean at locations away from the coastal sediment ^{228}Ra source, vertical mixing tends to dilute the ^{228}Ra concentration at the surface. Such a dilution effect is far less near the coast because of the small vertical concentration gradient of ^{228}Ra there, a result of the proximity to the sediment source throughout the water column. Therefore, we see there are two opposing effects on K_x: (1) ω_x which tends to make K_x larger and (2) vertical mixing which tends to lower the value of K_x. It would be possible to evaluate this vertical mixing effect quantitatively, if we had data on vertical profiles of ^{228}Ra in the surface ocean. Unfortunately, such data are not avialable at our stations. At present, we assume the two opposing effects to have more or less cancelled each other out, so that the modeled K_x values of *figure 4* adequately describe the horizontal mixing in the study area.

3.3. Near bottom ^{228}Ra profiles - vertical eddy diffusion coefficients

The non-Lapacian argument does not apply to vertical mixing, because here the elements travel over distances that are always small compared to the scales of observation (*figure 3*). The decrease of ^{228}Ra away from the surface mixed layer and away from bottom sediments in the water column can be explained by vertical eddy mixing and ^{228}Ra decay according to the equation [16, 20]:

$$K_z \frac{\partial^2 C}{\partial Z^2} - \lambda C = 0 \qquad (6)$$

where z = distance above the source regions; K_x is the apparent vertical eddy diffusivity; and other notations are as before. With the boundary condition that: $C = C_0$ at $z = 0$, and $C = 0$ at $z = \infty$, the solution is:

$$C = C_0 \exp(-\sqrt{\lambda/K_z}Z) \qquad (7)$$

This equation describes the decrease of ^{228}Ra with increasing z as an exponential function. Therefore, from the concentration gradient of ^{228}Ra in the water column, K_z can be estimated. It should be noted that the equation is applicable only within a single mixing regime. For example, we can not estimate K_z for the upper water column because the top two data points (at surface and 1000 m) belong to different water masses based on the T-S relationship (*figure 5*). In the bottom waters below 1000 m, the linearity in the T-S diagram suggests a well-characterised water mass for the application of the above equation. However, considering the absence of data between 1000 and 3000 m and the large uncertainty of the low ^{228}Ra activities at 1000 m, we would confine the modelling to the five data points more closely spaced near the bottom. Except for station 6, the derived K_z varies between 15 and 29 cm^2 s^{-1}, well within the range (5–100 cm^2 s^{-1}) observed elsewhere for open ocean bottom waters [4, 20]. However, the values thus deduced are distinctly larger than obtained from modern physical oceanographic work, such as the deliberate tracer release experiment conducted by Ledwell et al. [11]. One possibility to account for the difference would be lateral transport from the slope, as has been pointed out in previous work [1, 20]. The much higher K_z at station 6 (120 cm^2 s^{-1}) could also be caused by upwelling, as sug-

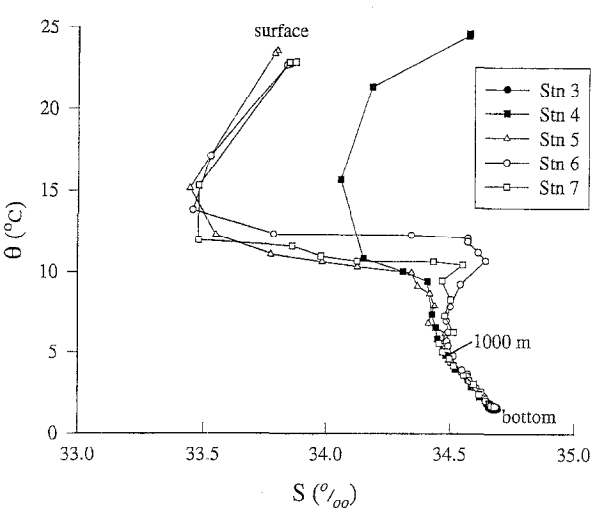

Figure 5. T-S diagrams at stations 3–7 showing a well-defined mixing regime below 1000 m.

gested by the ^{226}Ra data (*figure 2*), rather than by diffusion alone. Without a firm knowledge on hydrographic control, however, it is difficult to distinguish the effects of diffusion and advection in the water column. An attempt is made below based on ^{226}Ra to assess the importance of upwelling in the study area.

3.4 Radium budget in the northeast Pacific

Near-bottom distribution patterns of ^{226}Ra in seawater suggest that the northeast Pacific acts as a strong source, perhaps the strongest, for the oceanic presence of this isotope [8], a suggestion that is also consistent with model calculations of ^{226}Ra distributions on a global scale [3]. The implication is that ^{226}Ra supplied from the decay of ^{230}Th in deep-sea sediments and from water-column particulate dissolution in the region is transported out to other parts of the world ocean. It would be useful to test such an idea using the present data set, which provide an approximate E–W cross-section of the ^{226}Ra distribution in the northeast Pacific (*figure 2*). The test makes use of the ^{228}Ra data that give information on the near-bottom vertical diffusivities (*figure 3*) and on the surface ocean horizontal diffusion coefficients (*figure 4*).

We examine the problem by considering the mass balance of ^{226}Ra in the study area using a box model. As seen in *figure 6*, the box is divided into surface and deep layers, both bounded by station 7 in the east and station 3 in the west. Diffusive fluxes of ^{226}Ra into and out of the two layers are computed from Fick's first law, assuming that fluxes across the north and south boundaries of the box result in no net gain or loss of ^{226}Ra within the box. The material balance equations can be written as follows:

For the surface layer:

$$\frac{Z_s}{Y}\left[-\left(K_x\frac{\partial C}{\partial y}\right)_{s,E}-\left(K_x\frac{\partial C}{\partial y}\right)_{s,W}\right]$$

$$-\left(K_z\frac{\partial C}{\partial z}\right)_{1km}-\lambda\overline{C}_sZ_s=P \qquad (8)$$

For the deep layer:

$$\frac{Z_d}{Y}\left[-\left(K_x\frac{\partial C}{\partial y}\right)_{d,E}-\left(K_x\frac{\partial C}{\partial y}\right)_{d,W}\right]$$

$$-\left(K_z\frac{\partial C}{\partial z}\right)_{1km}-\left(K_z\frac{\partial C}{\partial z}\right)_{bottom}-\lambda\overline{C}_dZ_d=-R \qquad (9)$$

The notation in these equations is explained in the *figure 6* legend. The measured ^{226}Ra concentrations are averaged for each of the two layers to obtain $\overline{C}_s$ = 156 dpm m^{-3} and $\overline{C}_d$ = 350 dpm m^{-3}. The measured ^{226}Ra concentrations at each station are then interpolated to uniform depth intervals of 500 m, to give estimates for the horizontal concentration gradients at the eastern and western boundaries (from stations 7 and 3 and their respective neighboring stations), and for the vertical concentration gradients centred around 1 km (corresponding roughly to the main thermocline depth). To compute the horizontal ^{226}Ra fluxes across the two boundaries of the deep layer at stations 3 and 7, we use, respectively, K_x of 1×10^7 and 1×10^6 cm^2 s^{-1} [8, 9], and average horizontal gradients between 1 and 4 km of 3.7×10^{-5} and -6.0×10^{-5} dpm m^{-4}. For the surface box, we use K_x of 1 ×

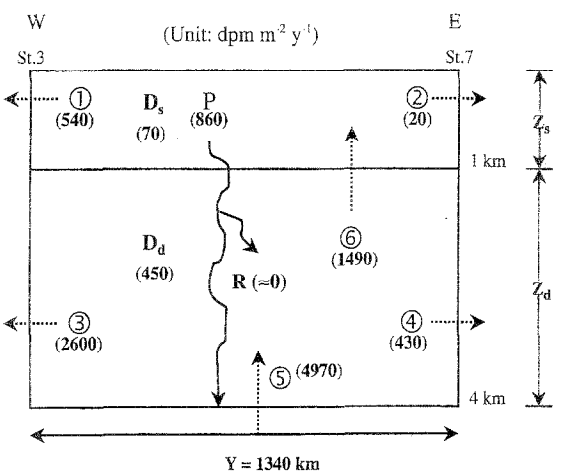

Figure 6. Two-box model depicting the balance of ^{226}Ra in the northeast Pacific.
Implicit in the model are the closure of water exchange with outside the box and the radium exchanges through eddy diffusion. The numerical values in parentheses are the computed ^{226}Ra fluxes in the unit of dpm m^{-2} y^{-1}. Note that all fluxes are expressed as equivalent flux per unit of horizontal area.

10^6 cm^2 s^{-1} for station 7 and K_x of 5×10^7 cm^2 s^{-1} for station 3. As these K_x values are derived from ^{228}Ra distributions in near-surface (~0 m depth) waters (*figure 4*), we combine them with the horizontal concentration gradients at 0 m of 0.47×10^{-5} dpm m^{-4} (station 3) and -0.77×10^{-5} dpm m^{-4} (station 7) to calculate the horizontal eddy diffusive fluxes. These flux estimates are assumed to be representative of the whole surface box.

The ^{226}Ra flux from the bottom refers to the sum of the flux from the sediment pore fluid and the flux due to dissolution of particulate ^{226}Ra at, or very close to, the sediment/water interface. As an input to the deep box, it is calculated as the mean diffusive fluxes at five stations shown in *figure 3*, each flux being the product of the ^{228}Ra-derived K_z and the local vertical concentration gradient based on the two bottom-most measured ^{226}Ra data points.

The computed Fickian horizontal and bottom fluxes of ^{226}Ra (expressed as dpm per unit area of seafloor per unit time) are shown in *figure 6* as fluxes #1 to #5, together with the output flux of radioactive decay in the two layers. With these fluxes and the average cross-thermocline concentration gradient of 0.12 dpm m^{-4} being fixed, there are three unknowns which remain to be solved from equations (5) and (6): K_z at 1 km, P, and R. However, previous studies [8, 9] have shown that negligible regeneration of ^{226}Ra takes place in the mid water column, hence $R \approx 0$. This enables us to assess the flux estimates of P and flux #6. The latter flux of 1490 dpm m^{-2}y^{-1} (*figure 6*) requires a vertical mixing coefficient for the thermocline of 3.8 cm^2 s^{-1}, almost three times larger than that obtained from the tritium distribution in the N. Pacific [12]. If this vertical mixing is parameterised in terms of advective transport as denoted by $\omega_z(\overline{C_d} - \overline{C_s})$ (where ω_z is the upwelling velocity, and $\overline{C_d}$ and $\overline{C_s}$ are the mean ^{228}Ra concentration in the deep and surface boxes, respectively), then ω_z in the study area averages 7.7 m y^{-1}, a value again higher than that generally quoted for the Pacific [3, 8].

How meaningful this is for the closure estimate is dictated by the uncertainties associated with fluxes #3 to #5. The closure flux of 1490 dpm m^2 y^{-1} (flux #6) for the deep box is 30 % of flux #5, the largest flux value in the ^{226}Ra-balance computation. However, the estimate for this flux from the seafloor is relatively well constrained. As mentioned above, it is the average of diffusive fluxes estimated from five stations. Influence of isopycnal mixing on the estimation of K_z at any of the five stations is expected to be cancelled out in the averaging process.

The box model calculation assumes a negligible net flux in the y (N–S) dimension. Is it realistic? In the absence of Ra data in this dimension, we may address this problem as follows. The closure flux (P) for the surface box of 860 dpm m^2 y^{-1} is larger than the fluxes of 540 and 20 dpm m^2 y^{-1} at the west and east boundaries (*figure 6*). If we take $K_x \approx K_y$ to attribute the 860 dpm m^2 y^{-1} flux to a net N–S (y) flux, it would require that the Ra concentration gradient in the y direction be larger than that in the x direction. This would not be expected from the distribution of shelf-sediments as the Ra source. Unless future measurements of $\partial C/\partial y$ show it to be significantly larger than $\partial C/\partial x$, we would take the omission of the y dimension in our box model calculation as a reasonable approximation.

Figure 2b and *3* indicate that the higher-than-average vertical transport in the area is reflected in the distributions of ^{226}Ra and ^{228}Ra near stations 5 and 6. The elevated ^{226}Ra concentrations in the vicinity of these stations serve to drive the export of this isotope through horizontal mixing. Our box model calculations show that this export, fueled by a strong bottom source and relatively high K_z and/or ω_z values, is particularly of sizable magnitude across the western boundary of the box. This feature is well manifested by the NE–SW decreasing trend of deep water ^{226}Ra concentrations in the Pacific [3].

4. CONCLUSION

The Ra isotopic data reported here for the northeast Pacific constitute one of the largest data sets outside the GEOSECS database. Mixing coefficients derived from the distribution of ^{226}Ra in surface and near-bottom waters generally agree with tracer-derived values reported previously. In order to maintain mass balance for ^{226}Ra, we found that vertical mixing through the permanent thermocline in the study area appears to be more rigorous than generally observed in the Pacific. It is suggested that this more pronounced vertical transport, coupled with horizontal mixing, serve to effectively export ^{226}Ra out of the northeast Pacific where an enhanced bottom source of ^{226}Ra exists.

Acknowledgments

The authors wish to thank Dr. J. W. Murray, Chief Scientist of the TT-145 cruise, and the officers and crew of *R/V T. G. Thompson* for their assistance during the cruise.

Mr. C.-C. Su assisted in the preparation of figures. The manuscript has benefited from discussion with Dr. Shangde Luo and from comments made by two anonymous reviewers. The work was supported in part by the U.S. National Science Foundation and the National Science Council of ROC.

REFERENCES

[1] Berelson W.M., Hammond D.E., Fuller C., Radon-222 as a tracer for mixing in the water column and benthic exchange in the southern California borderland, Earth Planet. Sci. Lett. 61 (1982) 41–54.

[2] Chung Y., Radium-barium-silica correlation and a two-dimensional radium model for the world ocean, Earth Planet. Sci. Lett. 49 (1980) 309–318.

[3] Chung Y., Craig H., ^{226}Ra in the Pacific Ocean, Earth Planet. Sci. Lett. 49 (1980) 293–308.

[4] Kaufman A., Trier R., Broecker W.S., Distribution of ^{228}Ra in the world ocean, J. Geophys. Res. 78 (1973) 8827–8848.

[5] Key R.M., Brewer R.L., Stockwell J.H., Guinasso N.L., Schink D.R., Some improved techniques for measuring radon and radium in marine sediments and in sea water, Mar. Chem. 7 (1979) 251–264.

[6] Knauss K.G., Ku T.-L., Moore W.S., Radium and thorium isotopes in the surface waters of the East Pacific and coastal Southern California, Earth Planet. Sci. Lett. 39 (1978) 235–249.

[7] Koczy F.F., Picciotto E., Poulaert G., Wilgain S., Mesure des isotopes du thorium dans l'eau de mer, Geochim. Cosmochim. Acta 11 (1957) 103–129.

[8] Ku T.-L., Huh C.-A., Chen P.-S., Meridional distribution of ^{226}Ra in the eastern Pacific along GEOSECS cruise tracks, Earth Planet. Sci. Lett. 49 (1980) 293–308.

[9] Ku T.-L., Luo S. New appraisal of Ra-226 as a large-scale oceanic mixing tracer. J. Geophys. Res. 99 (1994) 10255–10273.

[10] Ku T.-L., Luo S., Kusakabe M., Bishop J.K., ^{228}Ra-derived nutrient budgets in the upper equatorial Pacific and the role of "new" silicate in limiting productivity, Deep-Sea Res. 42 (1995) 479–497.

[11] Ledwell J.R., Watson A.J., Broecker W.S., A deliberate tracer experiment in Santa Monica Basin, Nature, 323 (1986) 322–324.

[12] Li Y.-H., Peng T.-H., Broecker W.S., The average vertical mixing coefficient for the oceanic thermocline, Tellus, 36B (1984) 212–217.

[13] Moore W. S., Measurement of ^{228}Ra and ^{228}Th in sea water, J. Geophys. Res., 74 (1969a) 694–704.

[14] Moore W. S., Oceanic concentrations of ^{228}Ra, Earth Planet. Sci. Lett., 6 (1969b) 437–446.

[15] Moore W. S., Radium-228: application to thermocline mixing studies, Earth Planet. Sci. Lett. 16 (1972) 421–422.

[16] Moore W.S., Sampling radium-228 in the deep ocean, Deep-Sea Res. 23 (1976) 647–651.

[17] Moore W.S., Reid D., Extraction of radium from natural waters using manganese-impregnated acrylic fibres, Deep-Sea Res. 23 (1973) 647–651.

[18] Moore W.S., Sackett W.M., Uranium and thorium series inequilibrium in sea water, J. Geophys. Res. 69 (1964) 5401–5405.

[19] Okubo A., Oceanic mixing diagrams, Deep-Sea Res. 18 (1971) 789–802.

[20] Sarmiento J.L., Feely H.W., Moore W.S., Bainbridge A.E., Broecker W.S., The relationship between vertical eddy diffusion and buoyancy gradient in the deep sea, Earth Planet. Sci. Lett. 32 (1976) 357–370.

[21] Somayajulu B.L.K., Goldberg E.D., Thorium and uranium isotopes in seawater and sediments, Earth Planet. Sci. Lett. 1 (1966) 387–391.

[22] Trier R.M., Broecker W.S., Feely H.W., (1972) Radium-228 profile at the second GEOSECS Intercalibration station, 1970 in the North Atlantic, Earth Planet. Sci. Lett. 16 (1972) 141–145.

[23] Yamada M., Nozaki Y., Radium isotopes in coastal and open ocean surface waters of the western North Pacific, Mar. Chem. 19 (1986) 379–389.